During hippocampal inactivation, grid cells maintain their synchrony, even when the grid pattern is lost

Noam Almog[1], Gilad Tocker[1,2ξ], Tora Bonnevie[3∞], Edvard Moser[3], May-Britt Moser[3] and Dori Derdikman[1‡]

[1]*Rappaport Faculty of Medicine and Research Institute, Technion – Israel Institute of Technology.*

[2]*Gonda Multidisciplinary Brain Research Center, Bar Ilan University.*

[3]*Kavli Institute for Systems Neuroscience and Centre for Neural Computation, Norwegian University of Science and Technology.*

‡Corresponding author. Email: derdik@technion.ac.il

ξ *Present address: Department of Neurobiology, Northwestern University, Evanston, Illinois.*

∞ *Present address: Department of Neuromedicine and Movement Science, Norwegian University of Science and Technology.*

Abstract

The means by which grid cells form regular, hexagonal spatial firing patterns has been an enigma since their discovery in the medial entorhinal cortex (MEC). Here we re-analyzed data from Bonnevie et al. (2013), in which the hippocampus was inactivated and grid cells were recorded in the MEC, to investigate whether grid cells form an intrinsic network in the MEC, or alternatively, inherit their network properties from external sources. Specifically, we examined temporal and spatial correlations in the firing times of simultaneously recorded grid cells before and during hippocampal inactivation. Our analysis revealed evidence of network coherence in grid cells even in the absence of hippocampal input to the MEC, both in regular grid cells and in those that became head-direction cells after hippocampal inactivation. This favors models which suggest that phase relations between grid cells in the MEC are dependent on intrinsic connectivity within the MEC.

Introduction

Since their discovery in the medial entorhinal cortex (MEC) (Hafting, Fyhn, Molden, Moser, & Moser, 2005) the location and means by which grid cells form their eponymous hexagonal spatial firing patterns

has been elusive. Modeling work has suggested that either grid cells are generated intrinsically in the MEC, for example by a continuous attractor network model (Burak & Fiete, 2009; Couey et al., 2013; Fuhs & Touretzky, 2006; Giocomo, Moser, & Moser, 2011; Moser, Moser, & Roudi, 2014; Zilli, 2012) or alternatively have their properties form through an interaction with another region, such as the hippocampus (Dordek, Soudry, Meir, & Derdikman, 2016; Kropff & Treves, 2008; Stachenfeld, Botvinick, & Gershman, 2017). To dissociate between these possibilities, we re-analyzed data from Bonnevie et al. (2013), who inactivated hippocampal input to the MEC, and found that under this condition, the grid pattern of individual grid cells deteriorated significantly or disappeared entirely. Here we investigated whether grid cells form an intrinsic network in the entorhinal cortex, or alternatively, inherit their spatial properties from external sources. Specifically, we examined correlations in the firing times of simultaneously recorded grid cells before and during hippocampal inactivation, including grid cells that acquired head directional tuning during inactivation. Our analysis yielded evidence of network coherence in grid cells even in the absence of hippocampal input to the MEC.

Results

We reanalyzed data from Bonnevie et al. (2013) in which grid cells were recorded before, during and after hippocampal inactivation (Figure 1A-C). A total of 301 well-separated cells were recorded in the MEC and parasubiculum across 40 sessions including pre-, during and post-hippocampal inactivation, with 2-18 simultaneously recorded cells per session. While the runs of pre- and post-inactivation were analyzed in their entirety, for runs during inactivation we used only the first 45 minutes, during which the most data were available across all recordings. The analysis showed similar effects on grid behavior in longer trials as in the first 45 minutes; the average grid score was -0.045±0.119 for the first 45 minutes and -0.049±0.087 for the remainder.

We searched for evidence of network activity between grid cells in the absence of hippocampal input. Hence, we examined spike time correlations and spatial firing correlations between simultaneously recorded cells whose gridness deteriorated during hippocampal inactivation (Figure 1D, 1E). To select only cells with high gridness before inactivation and low gridness during inactivation, we set a minimal grid score of 0.3 pre-inactivation and a maximum score of 0.2 during inactivation (Figure 1D). These thresholds were set subjectively to include the largest number of cells in our cohort, while ensuring typical grid cell activity pre-hippocampal inactivation and significantly less during hippocampal inactivation, based on the spatial firing pattern. The use of different thresholds (above 0.5 gridness pre-inactivation and below 0 gridness during inactivation) did not change our findings (see below).

The mean grid score of the selected cells was 0.85±0.33 pre-inactivation and -0.05±0.11 during inactivation. Additionally, to ensure that the same cell was not recorded on different electrodes, we removed any cells from a single recording session whose individual spike times overlapped within a 1ms window more than 6% of the time (this mostly removed cases with very large overlap that were clearly artefactual). The mean spike overlap after exclusion was 0.63%±0.82. Furthermore, we removed any cells whose grid score did not pass an n=250 shuffling significance test at a 99% threshold (see shuffling method below) pre-inactivation, and any cell whose grid score passed the same significance test during inactivation. In total, 63 of 301 cells from 17 of 41 recording sessions met our criteria (Figure 1D), producing 99 pairs of simultaneously recorded cells, on which the results of this study are based. In our cohort, firing rates decreased by 45.5% during inactivation, and returned to original levels post-inactivation (pre 2.20Hz±1.39, during 1.21Hz±0.94, and post 2.13Hz±1.17). However, overall, the firing rate did not seem to correlate to temporal or spatial correlations (Figs. 1B, 1C, 1E, S7).

Temporal correlations are maintained during loss of gridness

We found that several simultaneously recorded grid cell pairs consistently maintained temporal correlations even as their gridness deteriorated (Figure 2A, 2C). Compared to random shuffling, these correlations were statistically significant; 72%, 46%, and 68% of correlations passed the shuffling significance test pre-, during, and post-inactivation, respectively. Of the statistically significant correlations, 22%, 20%, and 21% were negative for the three respective recording phases, while 50%, 25%, and 47% were positive. Temporal correlations pre- vs. during inactivation were correlated at r=0.68 (Figure 3A, P<0.001), and pre- vs. post-inactivation were correlated at r=0.77 (Figure 3A, P<0.001). The strength of the correlation after inactivation demonstrated a slight negative dependence on the grid score (Figure 3-figure supplement 6). For comparison, the correlation coefficient of temporal correlations pre- vs. during for each cell from our cohort against each cell not from the same recording session (1854 pairs total) was r = 0.04 (P<0.11). Correlations of pre- vs. during inactivation were very similar when considering the period of the recordings after 45 minutes (Figure 3-figure supplement 5). Changing our pre- and during grid score thresholds did not change the results significantly: setting the thresholds of the grid score to 0.5 (from 0.3) pre- and 0.0 (from 0.2) during inactivation yielded pre/during temporal correlation of r = 0.73 (P<0.001). These correlations were also consistent across various spike train smoothing windows, in the range of 1ms-2000ms (Figure 2B and Figure 3-figure supplement 1). This suggests that the origin of the correlations was not a direct synaptic connection between cells, but rather recurrent network activity and dense connectivity. If the correlations had

resulted from direct synaptic connection, they would have been expected to have vanished as the temporal smoothing windows became larger, but they did not.

Spatial correlations are maintained during loss of gridness

To examine whether short-range spatial correlations were maintained also during hippocampal inactivation, we employed a similar method, which compared the correlation coefficient of the 2D firing rate maps at the same position (x,y = 0,0). Overall, spatial correlations did not persist as consistently as temporal correlations during hippocampal inactivation; however, some degree of persistence was present between simultaneously recorded cell pairs. Spatial correlations were correlated to each other pre-inactivation vs. during inactivation at r=0.54 (Figure 3C, P<0.001), while pre- vs. post-spatial correlations were correlated at r=0.82 (Figure 3C, P<0.001). For a control comparison, the correlation coefficient of spatial correlations pre- vs during inactivation for each cell from our cohort correlated against each other cell not from the same recording session, was much lower (r = 0.12). The shuffling significance test found that 54%, 22%, and 54% of spatial correlations were significant pre-, during, and post- inactivation, respectively. Of the correlations, 13%, 9%, and 13% were significantly negative for all three recording phases, respectively, while 41%, 13%, and 41% were positive (Figure 3D). Like temporal correlations, spatial correlations were not affected by smoothing up to 2000 ms of the spike train (Figure 3-figure supplements 2 and 3). Changing our pre- and during- grid score thresholds did not change the results significantly; setting the thresholds of grid score to 0.5 (from 0.3) pre- and 0.0 (from 0.2) during inactivation yielded a pre/during spatial correlation of r = 0.48 (P < 0.001). Although the statistical significance was lower overall for spatial correlations than for temporal correlations, the results for spatial correlations were consistent with those for temporal correlations. Additionally, plotting temporal and spatial correlations against each other demonstrated a clear linear relationship; the correlations of temporal to spatial correlations were r = 0.90, r = 0.84, and r = 0.91 for pre-, during, and post- inactivation, respectively (Figure 3-figure supplement 4).

Temporal correlations but not spatial correlations persisted during inactivation for grid-turned-head directional cells

In the original Bonnevie et al. (2013) study, a subset of grid cells became head direction cells during hippocampal inactivation. Cells within our cohort showed a bi-modal distribution of Rayleigh head-direction tuning scores during inactivation. This enabled selecting the cells that became head-direction cells (16 of the 63 cells in our cohort, from 3 of the 17 recording sessions; red dots in Figure 4C). We noticed that pairs from this subset (39/99) showed a lower rate of persistence of spatial correlation during inactivation. Figure 4A depicts an example of such group of cells from the same recording

session. Examining these head direction vs. non-head direction pair clusters separately, temporal correlations pre- and during inactivation were correlated to each other similarly in both clusters (r=0.72 vs. r=0.69, respectively, Figure 4D). The difference in correlation value (0.03) was higher than would result for only 6074 of 10000 randomly assigned clusters of the same size, implying that the two clusters were statistically indistinguishable with respect to temporal correlations. On the other hand, for spatial correlations, pre-inactivation compared to during inactivation, the correlation coefficient was r=0.68 in the non-head directional cluster, and much lower, r=0.32 (Figure 4E) in the head direction cluster. This difference was higher than would result for 9877 of 10000 randomly assigned clusters of the same size. However, a possible explanation entails the reduction in firing rate in the head-direction condition (Figure 4-figure supplement 1). In conclusion, while spatial correlations were probably less persistent in grid-turned-head direction cells, temporal correlations persisted equally in grid-turned-head direction cells during hippocampal inactivation, suggesting evidence, even in this subset, of the underlying network connectivity between the grid cells.

Discussion

This study reanalyzed data from Bonnevie et al. (2013), in which hippocampal input to the MEC was inactivated. The aim was to examine possible evidence of local grid cell functional connectivity. We found that despite the disappearance of the grid pattern of these cells during hippocampal inactivation, temporal correlations between grid cells remained, as did local spatial correlations, although to a lesser, yet still statistically significant degree. First, these findings assert that hippocampal input does not account for spatially and temporally correlated activity between grid cells. Second, the consistency of these correlations across a 1ms to 2000ms spike-time smoothing window indicates that this effect is not due solely to direct synaptic connectivity, but to recurrent network activity of dense networks in behavioral time-scales. Last, some grid cells became head-direction cells during hippocampal inactivation, and their spatial correlations were less dominant; nonetheless, temporal correlations persisted equally. Taken together, our findings indicate that grid cells are likely to have an underlying network structure in the MEC, which is compatible with an attractor manifold model of network behavior (Burak & Fiete, 2009; Couey, et al., 2013; Fuhs & Touretzky, 2006; Giocomo, et al., 2011; Moser, et al., 2014; Zilli, 2012), and not with feedforward models creating grid cells through summation of information from the hippocampus (Dordek, et al., 2016; Kropff & Treves, 2008; Stachenfeld, et al., 2017). We cannot preclude, though, the possibility that grid cells are formed through a different feedforward process, not involving the hippocampus, or that they are generated through a recurrent

loop involving information from both the hippocampus and the entorhinal cortex (Donato, Jacobsen, Moser, & Moser, 2017).

A network model for grid cell firing pattern at least strongly predicts, if not implicitly requires, a significant level of synchronicity in temporal firing between two networked grid cells (Moser, et al., 2014). The attractor manifold model for grid pattern generation predicts that even when the network is deprived of spatial input, in this case from the hippocampus, the activity pattern that is maintained (though no longer anchored to physical space) would cause nearby cells in the manifold to fire with high correlation, and more distant cells not to fire (Burak & Fiete, 2009; Dunn, Mørreaunet, & Roudi, 2014; Fuhs & Touretzky, 2006; Tocker, Barak, & Derdikman, 2015). This aligns with our observations of both correlated and anticorrelated activity during inactivation.

In addition to the evidence of network activity, we found that the distinct subset of cells that became head direction-tuned during inactivation, maintaine18d temporal but not spatial correlations during hippocampal inactivation. This subset of grid-turned-head-direction cells is likely defined by strong input from the retrosplenial cortex, or the pre- or para- subiculum, which also project into the MEC, and which dominate these cells' spatial tuning and firing time synchronization in the absence of input from the hippocampus (Clark & Taube, 2012). Because the conjunctive grid-head direction cells originated from recordings that did not contain pure grid cells, we did not observe direct evidence of a temporal correlation between grid cells that became head-direction cells and those that did not. Notably, both groups were similar in their temporal correlation values before and during inactivation, regardless of their differences in spatial correlations. This suggests that despite receiving additional spatial input, the grid cells that became head-direction cells were part of the grid-cell network.

Several other experiments have investigated grid cell activity when spatial input was curtailed, specifically following removal of visual input. In their original paper that described grid cells, Hafting et al. (2005) observed rat grid cells in darkness, and found that the grid pattern did not deteriorate. More recently, two studies, by Perez-Escobar et al. (2016) and Chen et al. (2016) that examined mouse grid cells in darkness reported that the grid pattern deteriorated without visual input. Furthermore, both studies found that significant temporal correlations were maintained during impaired spatial input to the entorhinal cortex, in accordance with our findings.

164 The steady synchronicity in our study suggests an underlying network structure in the MEC that is
165 responsible for grid cell formation. This corroborates the idea of an attractor manifold involved in grid
166 cell formation.

Methods

167 The following sections describe the acquisition of the original data from Bonnevie et al. (2013), and the
168 analytical methods we applied to the data. All code was written in Matlab (V. 2016a). The code was
169 uploaded to GitHub at github.com/noamza/muscimol.

170 Input data

171 Briefly, the original experiment by Bonnevie et al. (2013) was performed with eight male 3-5 month old
172 Long-Evans rats, with water available *ad libitum*. The rats were kept on a 12h light, 12h dark schedule
173 and tested in the dark phase. Rats were implanted with a microdrive connected to four tetrodes of
174 twisted 17-µm platinum-iridium wire; one bundle was implanted in the MEC in all rats, anteroposterior
175 0.4–0.5 mm in front of the transverse sinus, mediolateral 4.5–4.6 mm from the midline, and
176 dorsoventral 1.4–1.8 mm below the dura. Tetrodes were angled 10° in the sagittal plane. For
177 hippocampal inactivation, cannulae were implanted at a 30° angle in the posterior direction towards the
178 dorsal hippocampus; 0.24–0.30µl of the $GABA_A$ receptor agonist muscimol (5-aminomethyl-3-
179 hydroxyisoxazole) diluted in PBS was used to inactivate the hippocampus.

180 Rats were run in an open-field 100cm square arena polarized by a single white que card in an otherwise
181 black environment for a 20 min period, after which muscimol was infused. Subsequently, the firing rate
182 of all principal cells recorded in the dorsal CA1 region decreased rapidly, ~2.2 mm posterior and lateral
183 to the infusion site (82 cells, all of which were place cells), with firing rates dropping to 1% of the
184 baseline rate in 79% of the recorded cells within 20 minutes. Inactivation of the hippocampus had only
185 minimal impact on the behavior of the rats. Rats then ran for an average of 160 minutes in the open
186 field. After 6-24 hours, the rats were run for 20 minutes to check for cell recovery and grid stability.

187 Quantifying gridness and head direction selectivity

188 For this analysis, we were interested in specifically examining grid cells whose spatial firing pattern was
189 significantly degraded. To quantify this, we used the generally accepted measure of grid score, which
190 essentially measures the extent the cell's firing pattern repeats itself at 60° intervals on a two-
191 dimensional (2D) plane (how hexagonal the firing pattern is). The procedure undertaken to achieve this
192 calculation is as follows (based on the procedure described in (Sargolini et al., 2006; Tocker, et al., 2015):

First, a 2D map of neuron spiking was generated by creating a matrix where the index [i, j] represents the location in the arena, and the value represents the number of spikes in that location. The arenas selected for our data were of dimensions 100cm x 100cm; we binned our activity by 2cm x 2cm intervals. The equivalent matrix for time spent at each location was also created. These two matrixes were divided by each other element-wise, creating a matrix of firing rates at each location bin.

Next, a 2D spatial autocorrelation was performed on the rate map matrix (based on the one described in Hafting et al. (2005)). Firing fields were identified using a method that treated the smoothed (2D Gaussian smoothing with σ=2) autocorrelation matrix as an image, and identified distinct regions bounded by a given pixel value of *r* in all 8 directions whose external values are all less than *r*. Typical grid cell autocorrelations have at least 6 firing fields, at approximately 60° intervals (Hafting, et al., 2005). Cells whose autocorrelation did not create 6 distinct firing fields for calculating the anulus using the above method were set to a default grid score of 0. Typical grid cell activity was manifested as equidistant firing fields at 60° intervals from each other.

The final step in calculating the grid score was to create a ring around the center of the smoothed autocorrelation (2D Gaussian smoothing with σ=2), with an inner radius small enough to contain the innermost firing field, and the outer radius large enough to contain the outermost edge of the sixth closest field. Next, the ring was rotated 60° and correlated to the original. This value was then subtracted by the value of the ring correlated at a 30° rotation. Since both correlations have values in the range of [-1,1], the range of grid scores is [-2, 2].

A Rayleigh score from 0 to 1 was used to quantify head directionality of cells, similar to that described in Tocker et al. (2015).

Cell pair correlations

To quantify temporal correlations between cells, we calculated the Pearson correlation of their spike trains (lag = 0ms). For spatial correlations, a 2D Pearson correlation of the rate maps (see Quantifying Gridness) was performed and compared at [0,0]. Smoothing was done on the spike trains prior to both temporal and spatial correlations using a moving average window of 25ms. Smoothing windows from 1ms to 1000ms had little or no impact on the correlation of results (Figure 3-figure supplement 2).

Shuffling to measure significance

To measure the statistical significance of the correlations, we employed a shuffling method in which spike trains were randomly shifted cyclically n times (n=1000 unless stated otherwise) and their

correlations recalculated. Correlations were considered significant if they were in the 99th percentile when compared to the shuffled correlations. Positive and negative correlations were determined by sorting the correlation values in ascending and descending order, respectively, before determining their percentiles. A correlation in the 99th percentile, with values sorted in descending order, was considered a negative correlation; and values sorted in ascending order were considered a positive correlation.

Acknowledgements

We thank Cindy Cohen for proofreading. We thank Chen Elbak and Irina Reiter for help with experiment administration. We thank members of the Derdikman lab for fruitful discussions.

Funding

The research was supported by the Israel Science Foundation personal grants #955/13, #2344/16 and #2655/18, by a Rappaport Institute grant, by the Allen and Jewel Prince Center for Neurodegenerative Disorders of the Brain grant, and by a joint Technion-Weizmann Adelis foundation grant.

Conflict of Interest Statement

The authors declare that the research was conducted in the absence of any commercial or financial relationships that could be construed as a potential conflict of interest.

References

Bonnevie, T., Dunn, B., Fyhn, M., Hafting, T., Derdikman, D., Kubie, J. L., . . . Moser, M.-B. (2013). Grid cells require excitatory drive from the hippocampus. *Nature Neuroscience, 16*(3), 309-317.

Burak, Y., & Fiete, I. R. (2009). Accurate path integration in continuous attractor network models of grid cells. *PLoS computational biology, 5*(2), e1000291.

Chen, G., Manson, D., Cacucci, F., & Wills, T. J. (2016). Absence of visual input results in the disruption of grid cell firing in the mouse. *Current Biology, 26*(17), 2335-2342.

Clark, B. J., & Taube, J. S. (2012). Vestibular and Attractor Network Basis of the Head Direction Cell Signal in Subcortical Circuits. [Review]. *Frontiers in Neural Circuits, 6*. doi: 10.3389/fncir.2012.00007

Couey, J. J., Witoelar, A., Zhang, S.-J., Zheng, K., Ye, J., Dunn, B., . . . Witter, M. P. (2013). Recurrent inhibitory circuitry as a mechanism for grid formation. [10.1038/nn.3310]. *Nat Neurosci, 16*(3), 318-324. doi: http://www.nature.com/neuro/journal/v16/n3/abs/nn.3310.html#supplementary-information

Donato, F., Jacobsen, R. I., Moser, M.-B., & Moser, E. I. (2017). Stellate cells drive maturation of the entorhinal-hippocampal circuit. *Science, 355*(6330), eaai8178. doi: 10.1126/science.aai8178

Dordek, Y., Soudry, D., Meir, R., & Derdikman, D. (2016). Extracting grid cell characteristics from place cell inputs using non-negative principal component analysis. [JOUR]. *eLife, 5*, e10094. doi: 10.7554/eLife.10094

Dunn, B., Mørreaunet, M., & Roudi, Y. (2014). Correlations and functional connections in a population of grid cells. *arXiv preprint arXiv:1405.0044*.

Fuhs, M. C., & Touretzky, D. S. (2006). A spin glass model of path integration in rat medial entorhinal cortex. *Journal of Neuroscience, 26*(16), 4266-4276. doi: Doi 10.1523/Jneurosci.1353-05.2006

Giocomo, Lisa M., Moser, M.-B., & Moser, Edvard I. (2011). Computational Models of Grid Cells. *Neuron, 71*(4), 589-603.

Hafting, T., Fyhn, M., Molden, S., Moser, M.-B., & Moser, E. I. (2005). Microstructure of a spatial map in the entorhinal cortex. *Nature, 436*(7052), 801.

Kropff, E., & Treves, A. (2008). The emergence of grid cells: Intelligent design or just adaptation? *Hippocampus, 18*(12), 1256-1269.

Moser, E. I., Moser, M.-B., & Roudi, Y. (2014). Network mechanisms of grid cells. *Philosophical Transactions of the Royal Society B: Biological Sciences, 369*(1635), 20120511.

Perez-Escobar, J. A., Kornienko, O., Latuske, P., Kohler, L., & Allen, K. (2016). Visual landmarks sharpen grid cell metric and confer context specificity to neurons of the medial entorhinal cortex. *eLife, 5*, e16937.

Sargolini, F., Fyhn, M., Hafting, T., McNaughton, B. L., Witter, M. P., Moser, M. B., & Moser, E. I. (2006). Conjunctive representation of position, direction, and velocity in entorhinal cortex. *Science, 312*(5774), 758-762. doi: 312/5774/758 [pii]10.1126/science.1125572

Stachenfeld, K. L., Botvinick, M. M., & Gershman, S. J. (2017). The hippocampus as a predictive map. *Nature Neuroscience, 20*(11), 1643.

Tocker, G., Barak, O., & Derdikman, D. (2015). Grid cells correlation structure suggests organized feedforward projections into superficial layers of the medial entorhinal cortex. *Hippocampus, 25*(12), 1599-1613. doi: 10.1002/hipo.22481

Zilli, E. A. (2012). Models of grid cell spatial firing published 2005-2011. [Review]. *Frontiers in Neural Circuits, 6*. doi: 10.3389/fncir.2012.00016

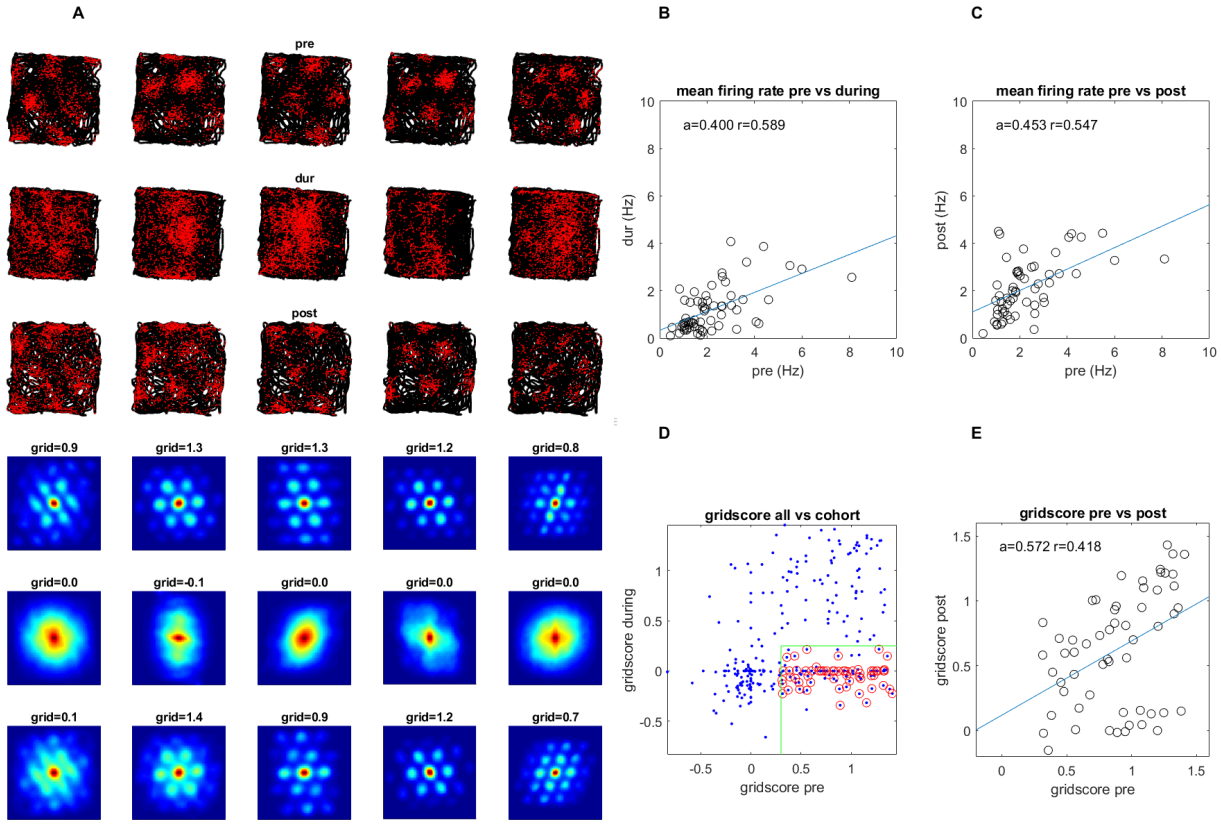

Figure 1. A survey of the grid cell population included in the study. Recordings were made pre-, during, and post-injection of muscimol to the hippocampus. (**A)** A sample group of 5 simultaneously recorded grid cells, one cell per column. The first three plots in each column show the location of a single cell firing (red) along the rat's trajectory (black) in a square arena pre-, during, and post-hippocampal inactivation, respectively. The last three plots in each column show the autocorrelation of the firing rate map and the grid score of that session pre-, during, and post inactivation. (**B**) The mean firing rate for the 63 grid cells included in the study pre- vs. during inactivation. (**C**) Same as (B) but for pre- vs. post-inactivation. (**D**) The grid score of all cells in the dataset vs. those included in the study. Green lines show the score thresholds used to select the cells for the cohort, red circles show the cells that were ultimately included in the study after applying grid score and other criteria (note that cells whose grid scores could not be calculated were set to 0, see methods). (**E**) Grid score pre- and post- inactivation of the cells included in the study.

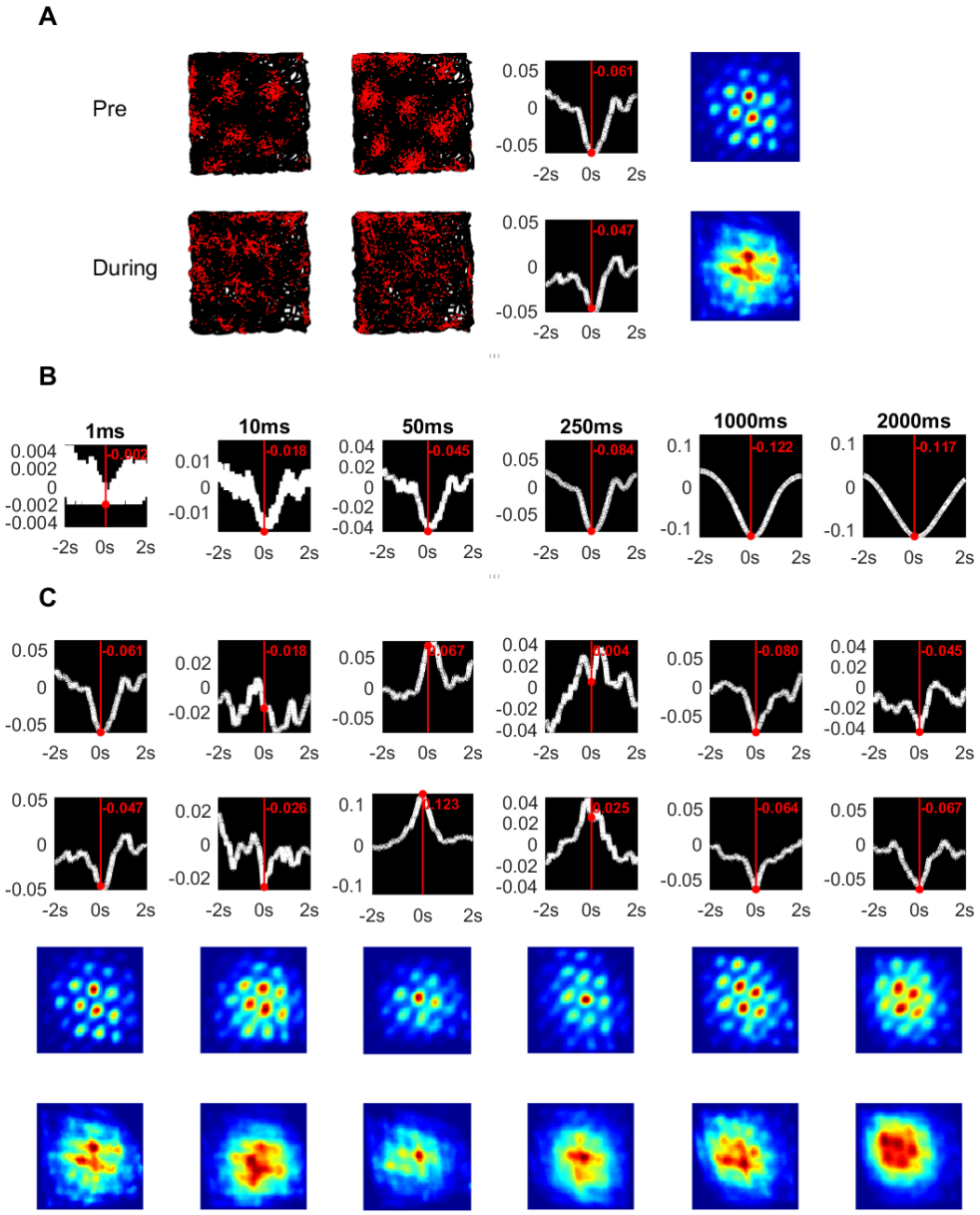

Figure 2. Temporal and spatial cross correlations of simultaneously recorded grid cells pre- and during hippocampal inactivation. (**A**) An example of a pair of simultaneously recorded grid cells (columns 1, 2) and their temporal and spatial cross correlation. The rows show pre- and during inactivation data, respectively. (**B**) The effect of smoothing the spike train on the temporal cross correlation using different window lengths with a moving average filter. (**C**) The temporal and spatial cross correlations of cell pairs of an entire group of simultaneously recorded grid cells. Rows 1, 2 show temporal cross correlations pre- and during inactivation; rows 3, 4 show the same for spatial correlations.

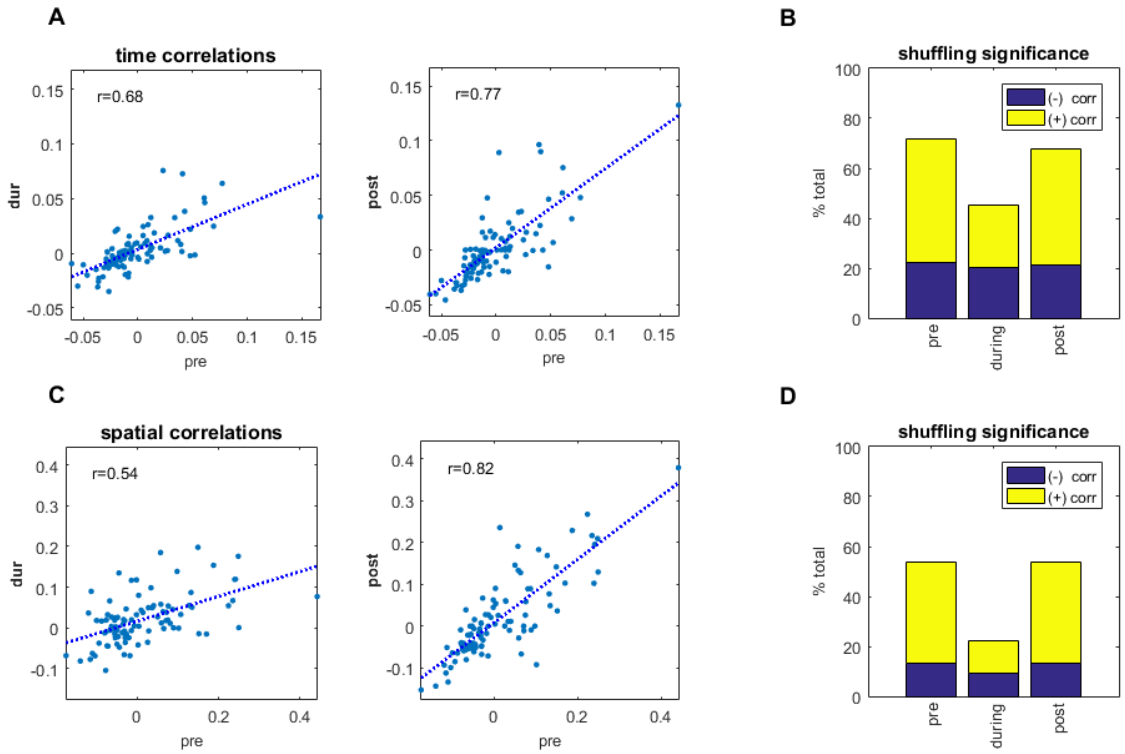

Figure 3 (with 6 supplements). Temporal and spatial cross correlations pre- and during inactivation. (**A**) Temporal cross correlations pre- and during inactivation, and also pre- and post- inactivation (**B**) Proportions of significant temporal cross correlations, according to shuffling measures, pre-, during, and post-inactivation, including the sign (positive, negative) of the correlation value. (**C**) Same as (A) but for spatial cross correlations of the firing pattern in the arena at [0,0]. (**D**) Same as (B) but for spatial cross correlations of the firing pattern in the arena at [0,0].

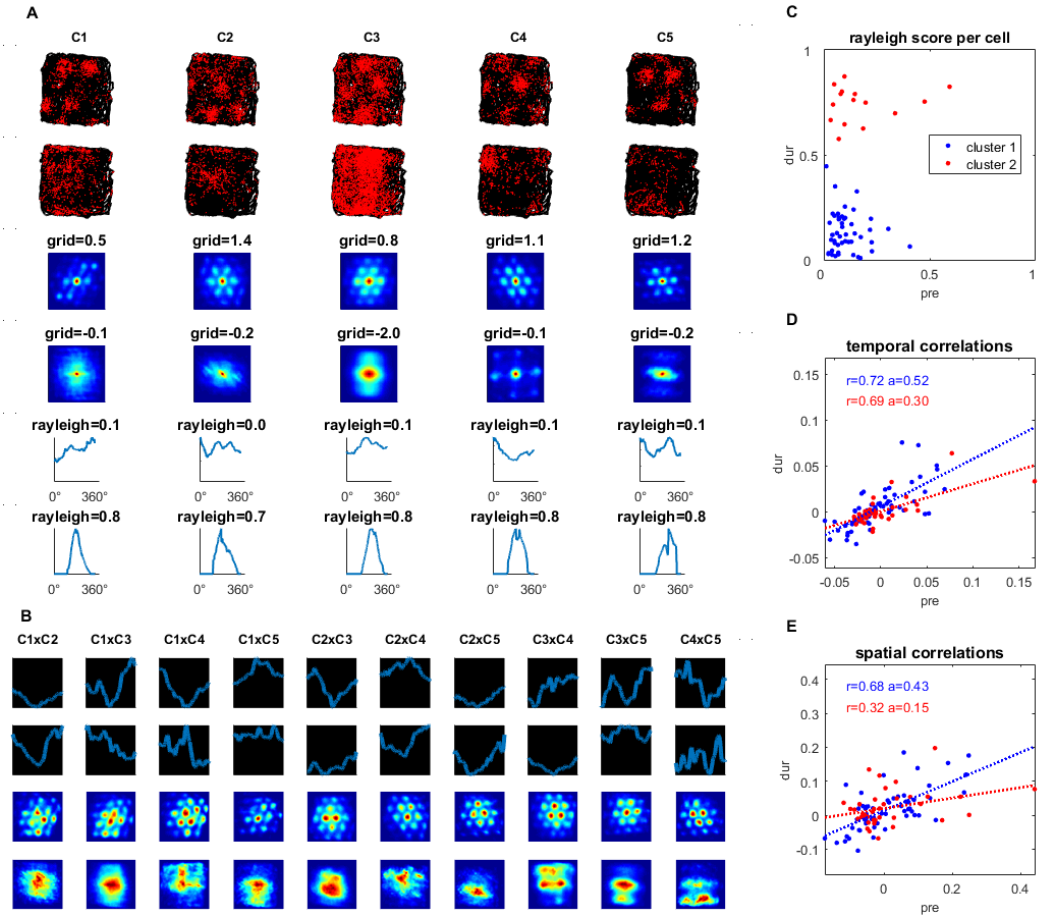

Figure 4 (with 1 supplement). Simultaneously recorded grid cells that became head directional during hippocampal inactivation. (**A**) A sample group of 5 simultaneously recorded grid cells, one cell per column. The first two plots in each column show the location of a single cell firing (red) along the rat's trajectory (black) in a square arena pre- and during hippocampal inactivation. Next, two plots show the autocorrelation of the firing rate map and the associated grid score pre- and during inactivation. The last two plots in the column show the firing rate by head direction for an associated Rayleigh Score, pre and during inactivation. (**B**) Temporal and spatial correlations for each cell pair of the group, pre- and during inactivation by column. For temporal correlations (rows 1 and 2), the y-axis represents the correlation value and the x-axis the time lag, ranging from -2s to 2s; no lag, (0s lag) is midway on the x-axis. (**C**) Rayleigh scores pre- and during inactivation for all cells in the cohort clustered by low head directionality (Rayleigh Score < 0.55) during inactivation (blue) and high head directionality (Rayleigh Score > 0.55, red) (**D**) Temporal correlations pre- and during inactivation grouped by head directionality clusters defined in (C), with the correlation coefficient and trendline slope. (**E**) Same as (D) but for spatial correlations.

Supplement Figures

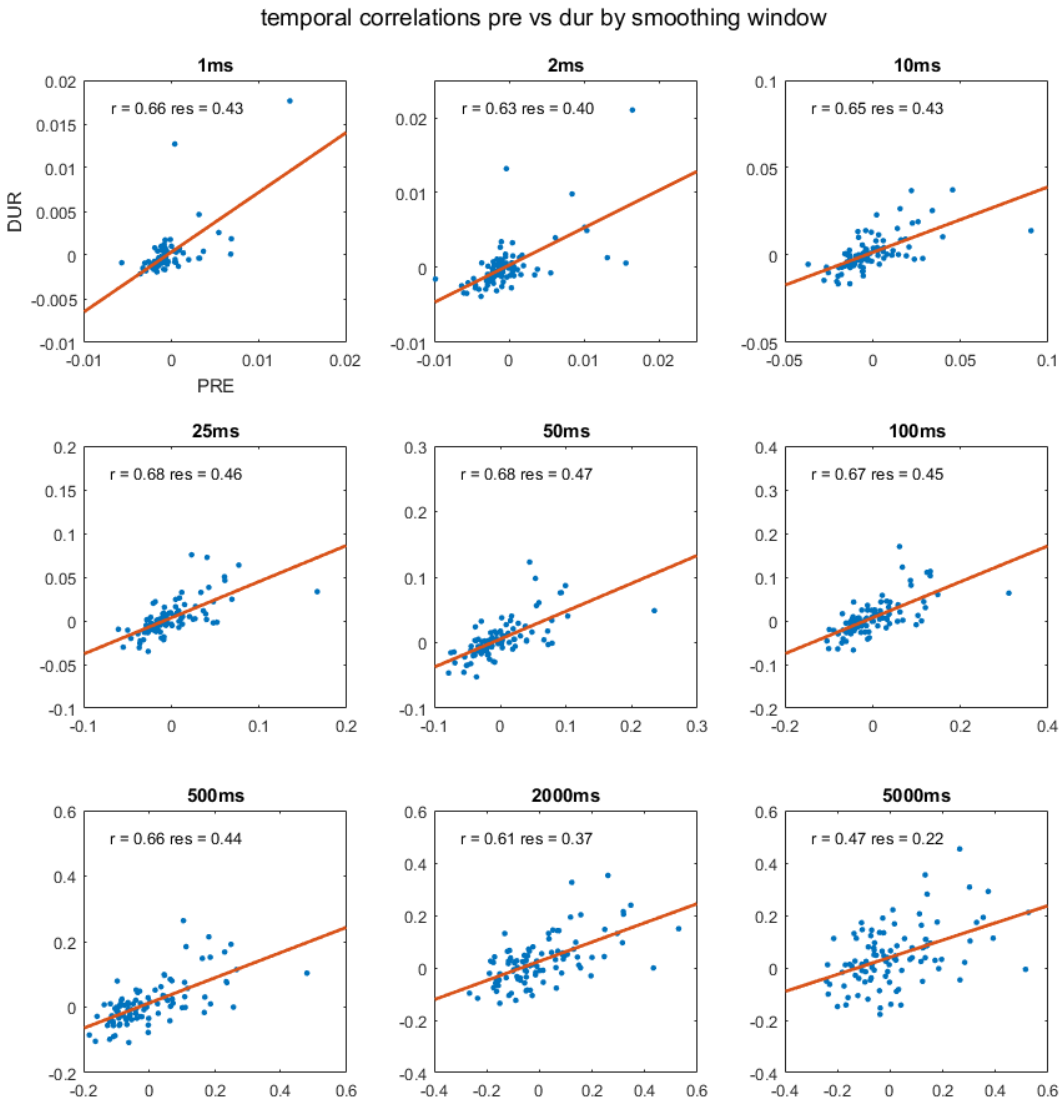

Figure 3-figure supplement 1. A plot of temporal cross correlations of the cells in our cohort pre- vs. during hippocampal inactivation, across nine smoothing windows, from 1ms to 5000ms. Spike trains were smoothed using a moving average.

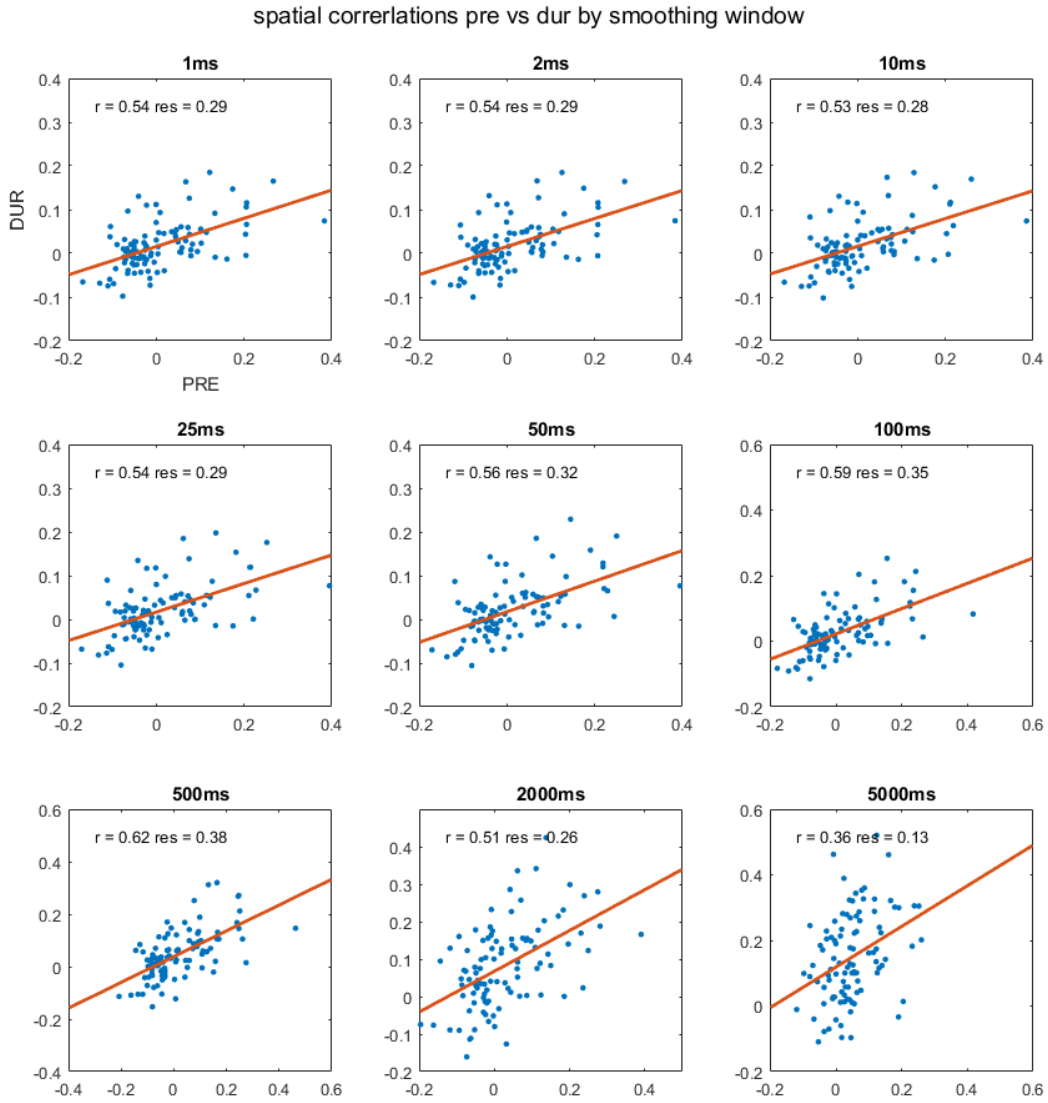

Figure 3-figure supplement 2. A plot of spatial cross correlations at [0,0] of the cells in our cohort pre- vs. during hippocampal inactivation, across nine smoothing windows, from 1ms to 5000ms. Spike trains were smoothed using a moving average.

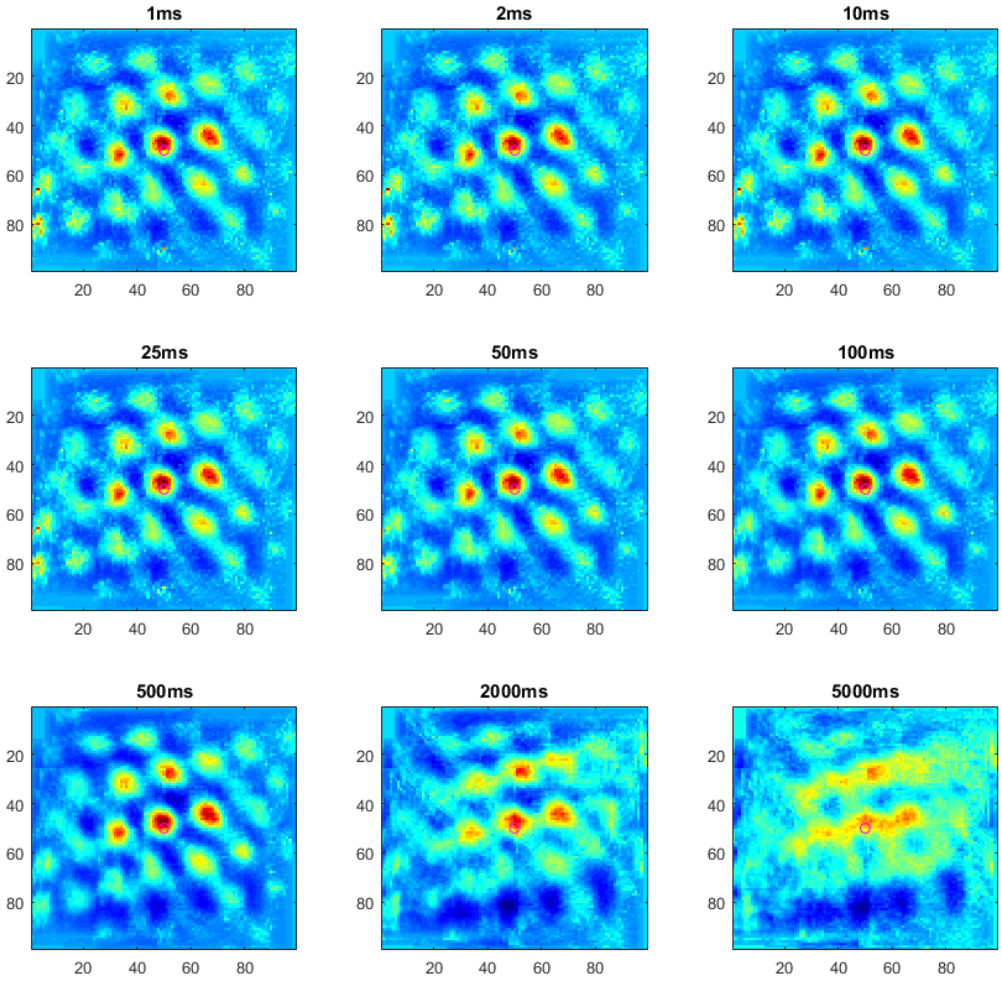

Figure 3-figure supplement 3. A single example of spatial cross correlation between two grid cells, pre-hippocampal inactivation across nine smoothing windows, from 1ms to 5000ms. Spike trains were smoothed using a moving average.

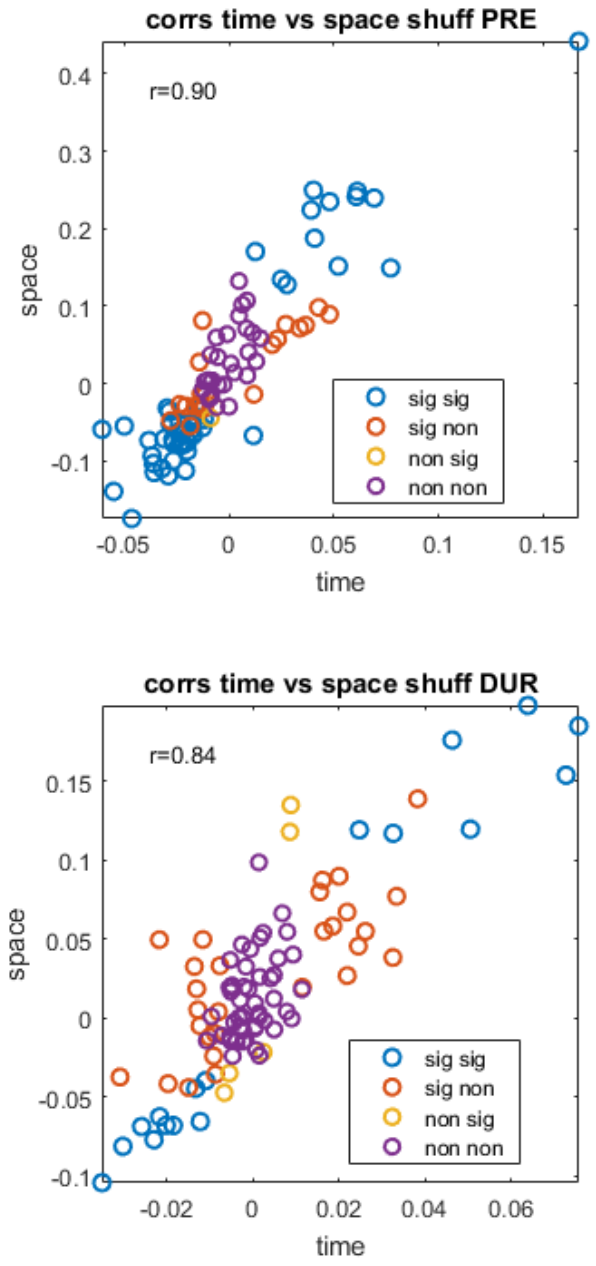

Figure 3-figure supplement 4. Temporal correlations plotted against spatial correlations for the cell pairs in our cohort, highlighted by significance pre- (top) and during inactivation (bottom). The legend shows temporal significance followed by spatial significance, with either being significant (sig) or non-significant (non).

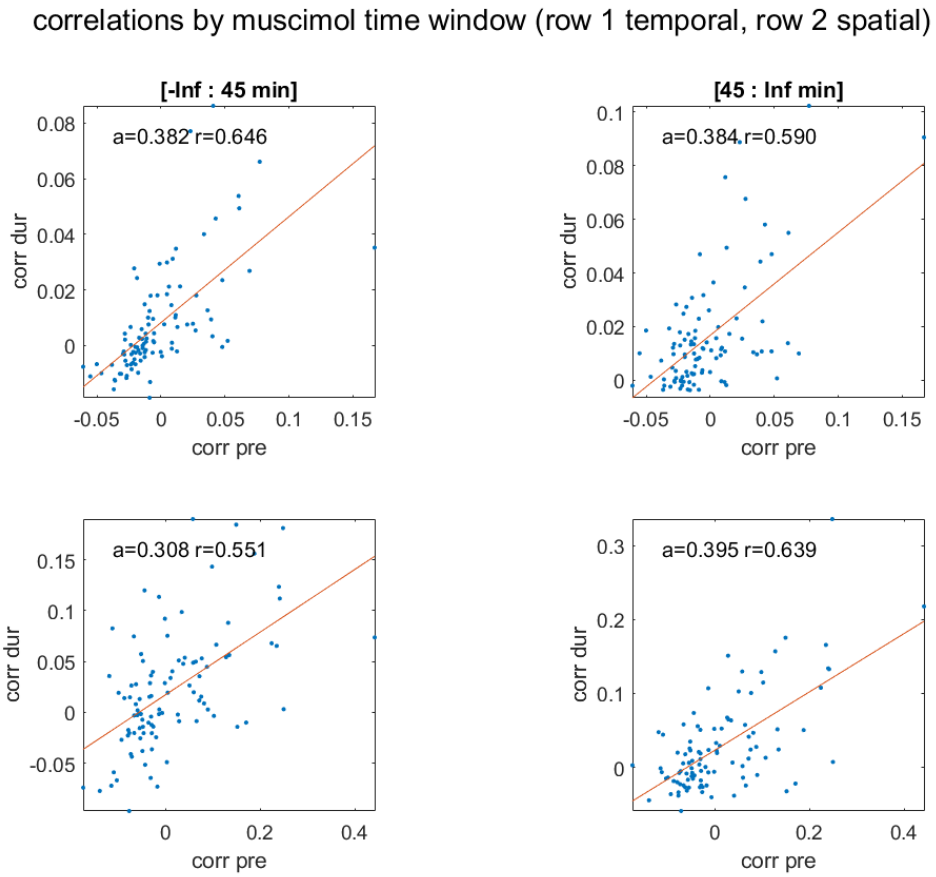

Figure 3-figure supplement 5. Temporal correlations pre-inactivation plotted against the recording period during inactivation used in this analysis; all recordings after muscimol injections are up to 45 minutes (top left) and all remaining recordings after 45 minutes (top right) of the muscimol recording session, including slope of the regression line (a) and the Pearson correlation (r). The second row shows the same plots for spatial correlations. Note: because recordings had different starting and ending times, [-Inf, Inf] are used to signify the start and end of the recording time; on average, recordings started 10 minutes after the injection and ended 115 minutes after the injection.

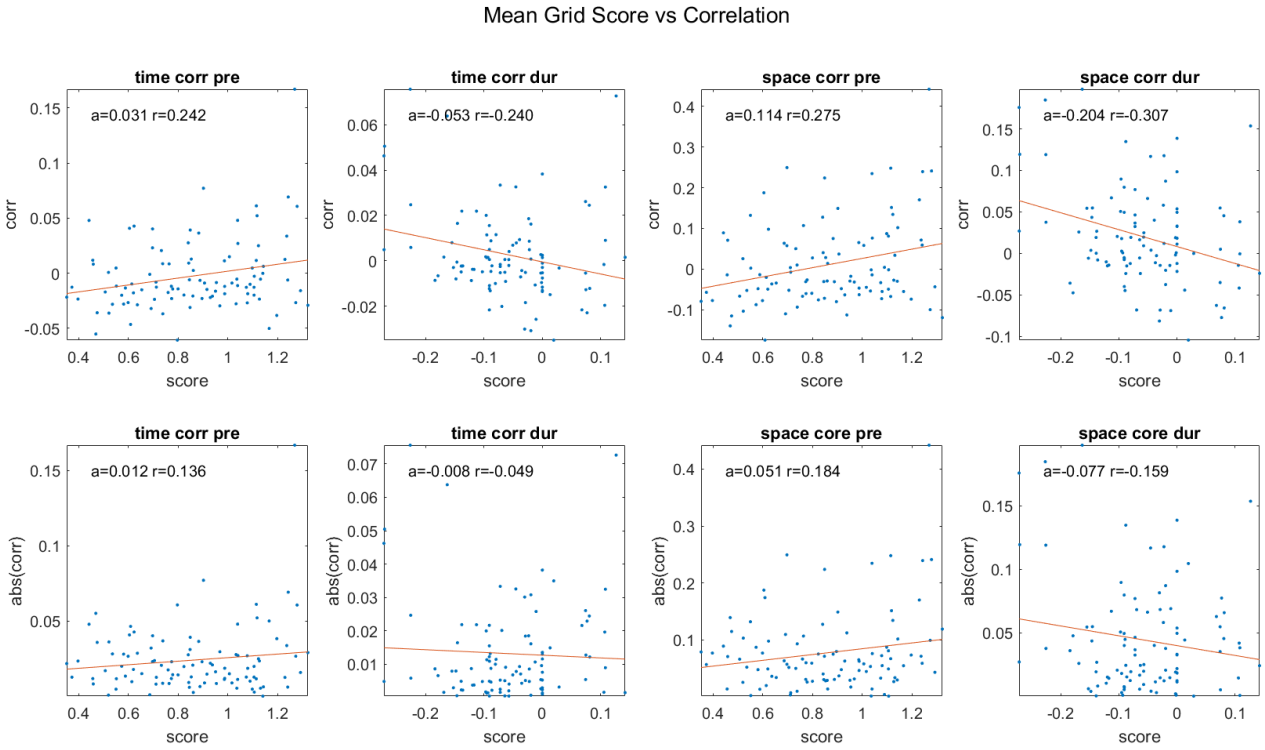

Figure 3-figure supplement 6. Temporal and spatial correlations for cell pairs pre- and during inactivation plotted against their average grid score, including the slope of the regression line (a) and the Pearson correlation (r). The second row shows the same plots for absolute correlation values.

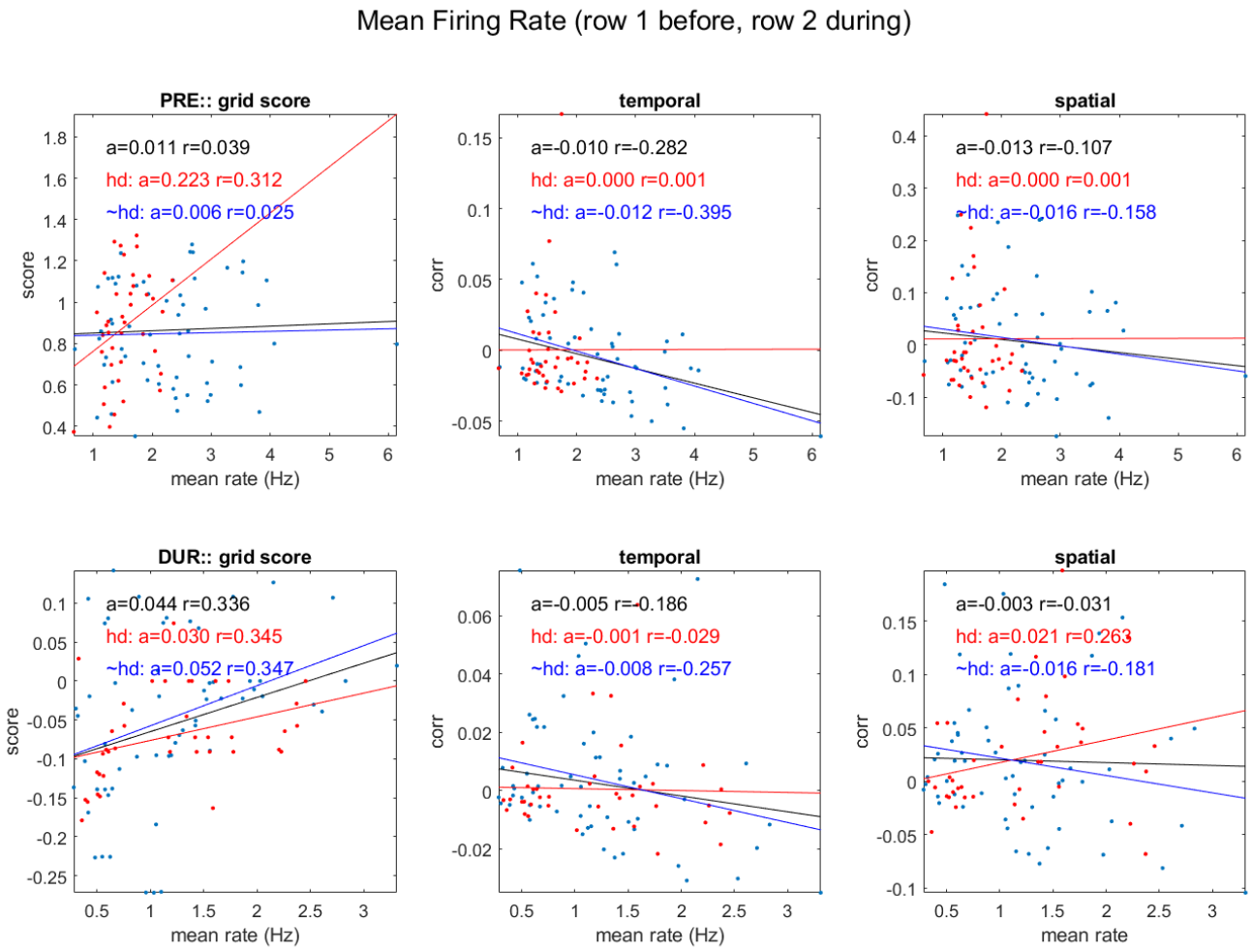

Figure 4-figure supplement 1. The mean firing rate of cell pairs plotted against their mean grid score, temporal and spatial correlations, pre- and during inactivation, rows (1 and 2, respectively), grouped by cells with head directionality during inactivation (red), without (blue), and all (black), including the slope of the regression line (a) and Pearson correlation (r).